



Zheng, Y., Pancost, R., Naafs, D., Li, Q., Liu, Z., & Yang, H. (2018). Transition from a warm and dry to a cold and wet climate in NE China across the Holocene. *Earth and Planetary Science Letters*, 493, 36-46.
<https://doi.org/10.1016/j.epsl.2018.04.019>,
<https://doi.org/10.1016/j.epsl.2018.04.019>

Peer reviewed version

License (if available):
CC BY-NC-ND

Link to published version (if available):
[10.1016/j.epsl.2018.04.019](https://doi.org/10.1016/j.epsl.2018.04.019)
[10.1016/j.epsl.2018.04.019](https://doi.org/10.1016/j.epsl.2018.04.019)

[Link to publication record in Explore Bristol Research](#)
PDF-document

This is the author accepted manuscript (AAM). The final published version (version of record) is available online via Elsevier at <https://www.sciencedirect.com/science/article/pii/S0012821X1830222X>. Please refer to any applicable terms of use of the publisher.

University of Bristol - Explore Bristol Research

General rights

This document is made available in accordance with publisher policies. Please cite only the published version using the reference above. Full terms of use are available:
<http://www.bristol.ac.uk/pure/about/ebr-terms>

23 changes in mean annual air temperature and peat soil moisture across the last ~ 13,000
24 year BP using samples from the Gushantun and Hani peat, located in NE China. Our
25 approach is based on the distribution of bacterial branched glycerol dialkyl glycerol
26 tetraethers (brGDGTs) and the abundance of the archaeal isoprenoidal (iso)GDGT
27 crenarchaeol. Using the recently developed peat-specific $MAAT_{peat}$ temperature
28 calibration we find that NE China experienced a relatively warm early Holocene
29 (~5-7 °C warmer than today), followed by a cooling trend towards modern-day values
30 during the mid- and late Holocene. Moreover, crenarchaeol concentrations,
31 brGDGT-based pH values, and the distribution of 6-methyl brGDGTs, all indicate an
32 increase in soil moisture content from the early to late Holocene in both peats, which
33 is largely consistent with other data from NE China. This trend towards increasing
34 soil moisture/wetter conditions across the Holocene in NE China records contrasts
35 with the trends observed in other parts of the EASM region, which exhibit an early
36 and/or mid-Holocene moisture/precipitation maximum. However, the Holocene soil
37 moisture variations and temperature-moisture relationships (warm-dry and cold-wet)
38 observed in NE China are similar to those observed in the core area of arid central
39 Asia which is dominated by the westerlies. We therefore propose that an increase in
40 the intensity of the westerlies across the Holocene, driven by increasing winter
41 insolation, expanding Arctic sea ice extent and the enhanced Okhotsk High, caused an
42 increase in moisture during the late Holocene in NE China.

43 Keywords: Peatland, GDGTs, Holocene hydrological evolution, air temperature, NE
44 China

46 **1. Introduction**

47 Climate in northeastern (NE) China is influenced by the interplay of different
48 atmospheric circulation patterns, predominantly the Asian monsoon system and the
49 northern-part of the Westerlies. The climate evolution in the region since the last
50 deglacial period has been reconstructed using various types of paleoclimatic archives,
51 such as lake sediments (e.g., Stebich et al., 2015; Zhou et al., 2016), peats (e.g., Zhou
52 et al., 2010; Zheng et al., 2017), and speleothem oxygen isotope records (e.g., Wu et
53 al., 2011). Several of these paleoclimatic studies have suggested that the climate of
54 this region since the last deglaciation differed from that of other East Asian monsoon
55 regions (e.g., Zhou et al., 2010; Stebich et al., 2015; Zheng et al., 2017).

56 Although these paleoclimate studies have improved our understanding of Holocene
57 climate and environmental change, the various reconstructed patterns of hydrological
58 change in NE China are inconsistent. For example, using *n*-alkane ratios in peat, Zhou
59 et al. (2010) suggested that NE China was characterized by a dry early Holocene
60 (~10.5 to 6 ka), attributed to enhanced evaporation caused by high sea surface
61 temperatures (SSTs) from the nearby Japan Sea, and a wet late Holocene (after ~6 ka).
62 This is consistent with pollen records from lake sediments from the Sihailongwan
63 Maar and Tianchi lake (see compilation of Fig. 1) that indicate wettest conditions after
64 5 ka (Stebich et al., 2015; Zhou et al., 2016). However, a climatic evolution from a
65 dry early Holocene to a wet late Holocene is unexpected, because the intensity of the

66 EASM is controlled by local summer insolation, with high insolation warming the
67 continent and leading to a stronger EASM (Wang et al., 2005a; Wang et al., 2005b).
68 Summer insolation was highest during the early Holocene and decreased since then
69 (Berger and Loutre, 1991). Indeed, there are other records from the region that
70 indicate a wet early Holocene and dry late Holocene (Li et al., 2017), more in-line
71 with the expected evolution of the EASM based on the local insolation. The
72 contrasting response recorded in different proxies and in different regions indicates
73 that the climatic evolution of NE China and especially the EASM across the Holocene
74 remains poorly constrained. This highlights a fundamental gap in our understanding
75 of the processes and mechanisms that drive the expression of the Monsoon in NE
76 China.

77 Over the last decade, peats have become an important archive for the reconstruction
78 of terrestrial climate change in Asia (e.g., Barber et al., 2003; Xie et al., 2004; Hong et
79 al., 2005; Zheng et al., 2007, 2015, 2017; Dise, 2009). The rate of peat accumulation
80 and water table position are sensitive to changes in precipitation and temperature
81 (Barber et al., 2000; Ise et al., 2008). Peat deposits are widespread in NE China and
82 can extend back into the last deglaciation, representing the potential to constrain the
83 deglacial evolution of climate. Previous peat-based palaeoclimate studies in NE China
84 have focused predominantly on the Hani peatland using a range of proxies including
85 *n*-alkane δD and $\delta^{13}C$ values (Seki et al., 2009; Yamamoto et al., 2010), peat cellulose
86 $\delta^{13}C$ and $\delta^{18}O$ records (Hong et al., 2005; Hong et al., 2009), compositional changes
87 in *n*-alkanes, *n*-alkanoic acids and *n*-alkanols (Zhou et al., 2010), *n*-alkan-2-one

88 distributions (Zheng et al., 2011), glycerol dialkyl glycerol tetraethers (GDGTs)
89 (Zheng et al., 2017), and microfossil analysis (Schröder et al., 2007). However,
90 biomarker records are currently lacking from other peats in NE China that span the
91 deglaciation such as the Gushantun peat deposits. Although pollen and grain sizes
92 have been used to reconstruct Holocene climate and vegetation changes in the
93 Gushantun peat (Liu et al., 1989; Zhao et al., 2015; Li et al., 2017), the temperature
94 and paleohydrological variations in this peatland during the Holocene are currently
95 unknown. To provide new information on the paleoclimate history of NE China, and
96 dynamics of the EASM, our study employs high temporal resolution (~100-200 year
97 resolution) paleoclimatic proxies based on the abundance and distribution of GDGTs,
98 similar to that of previous Holocene studies (Zheng et al., 2014, 2015, 2017).

99 There are two main classes of GDGTs and both are abundant in peat: i) branched
100 (br)GDGTs, membrane lipids of bacteria that occur ubiquitously in mineral soils and
101 peats (Weijers et al., 2006, 2007; Sinninghe Damsté et al., 2000; Naafs et al., 2017a),
102 and ii) isoprenoidal (iso)GDGTs, membrane lipids of Archaea that are present in
103 mineral soils and peat but typically dominate the GDGT pool in aquatic (marine)
104 settings (Schouten et al., 2000, 2013). At present 15 different brGDGTs have been
105 identified, bearing 0 to 2 extra methyl groups at either the C-5 or C-6 position and/or
106 up to two cyclopentane moieties (De Jonge et al., 2013, 2014). The distribution of
107 brGDGTs in mineral soils can be used to reconstruct past air temperatures and soil pH
108 (Weijers et al., 2007; Peterse et al., 2012; De Jonge et al., 2014; Naafs et al., 2017b).
109 Although most work on brGDGTs is based on mineral soils and lake sediments,

110 peat-specific temperature and pH calibrations have recently been developed (Naafs et
111 al., 2017a). The peat-specific proxies allow us to reconstruct temperature and pH
112 variations over the Holocene in the Gushantun peat sequence. In addition to brGDGTs,
113 changes in the relative abundance of crenarchaeol, a biomarker so far known only to
114 be biosynthesized by *Thaumarchaeota* (Sinninghe Damsté et al., 2002; Schouten et al.,
115 2013), have been used to identify past dry periods in peat (Zheng et al., 2015).

116 The GDGT-based records of temperature, pH, and aridity from the Gushantun and
117 Hani peat are compared with those from other sites in NE China, as well as other
118 Asian summer monsoon-dominated regions and arid central Asia such as the
119 Xingjiang region, in order to confirm that our data are representative of Holocene
120 hydrological and temperature evolution across NE China. Based on this, we offer new
121 perspectives on Holocene climate changes and mechanisms driving climate in NE
122 China.

123

124 **2. Material and methods**

125 *2.1 Study Site*

126 The Gushantun peat deposit (42°18'N, 126°17'E) is situated in Huinan County in
127 Jilin Province at an elevation of 500 m on the western flank of the Changbai
128 Mountains (Fig. 1; see Zheng et al. (2017) for precise location of the Hani peat). It is
129 surrounded by a basalt platform that is more than 600 m high. It is suborbicular with a
130 diameter of about 1 km and slopes from north to south. The ground is perennially

131 saturated with water, so a swampy, peat-forming environment has been sustained in
132 this region since the last deglaciation, and a sequence of peat of around 1-2 m in
133 average thickness (8-9 m in maximum thickness) has accumulated. At present, the
134 annual mean temperature is ~ 3 °C, with monthly mean temperatures that range from
135 -16 °C in January to 21 °C in July. The annual mean precipitation is about 700 mm
136 (Liu et al., 1989).

137 Our samples are from a 735 cm long core collected from near the center of the
138 Gushantun peat. The core consists of 655 cm of brown to dark brown peat containing
139 a large amount of non-degraded plant residue. Below 655 cm depth, the sediment is
140 grayish-green to dark brown mud, representing lacustrine depositional conditions.
141 After collection, the core was transported intact to the laboratory where it was
142 subsampled at 1-cm intervals. All samples were stored at -20 °C until analyses, and a
143 total of 93 samples were analysed for their GDGT distribution.

144

145 *2.2. Chronology of the peat core*

146 Sample pretreatment, AMS-target preparation and AMS measurement were all
147 conducted at the Xi'an AMS Laboratory. The pre-treatment of 8 peat samples for ^{14}C
148 dating was performed using the method of Zhou et al. (2002): plant fragments with a
149 size ranging from 90 to 300 μm were isolated from peats by wet sieving and then
150 subjected to an Acid-Alkali-Acid (HCl-NaOH-HCl) treatment. Two samples of total
151 organic carbon (TOC) from bulk mud sediments at the bottom of the lacustrine layers

152 was processed using 10% HCl to remove all carbonate content before graphitization
153 (Zhou et al., 2004). AMS-targets were prepared from the pretreated samples, which
154 were then placed with CuO powder into 9 mm quartz tubes, evacuated to $<10^{-5}$ torr,
155 and then combusted. The CO₂ was converted catalytically to graphite using Zn (Zn
156 powder with added Fe powder as a catalyst) (Slota et al., 1987). The calibrated ages
157 were obtained from the ¹⁴C ages using the Northern Hemisphere INTCAL13 curve
158 (Stuiver et al., 1993; Reimer et al., 2013). In order to produce the reliable ages for all
159 depths in the Gushantun peat core, we used Bayesian age-depth modeling software
160 Bacon (Blaauw et al., 2011) to estimate ages and uncertainties for each sample (Fig. 2
161 and Table 1). The model using a Bacon approach provides a chronological framework
162 for the past 13,000 years. Two samples were excluded as outliers based on a student-t
163 model (Blaauw et al., 2011). We also note that the shallowest sample, from 8 cm, has
164 a modern age, which could indicate mixture of carbon-ages in the peat profile, i.e. via
165 root production; in the absence of high resolution approaches such as wiggle matching,
166 these processes cannot be resolved and represent a small additional source of error in
167 our age model.

168

169 *2.3. GDGT extraction and analysis*

170 Freeze-dried, homogenized samples (including the Hani peat samples see Zheng et
171 al., 2017 for details) were extracted ultrasonically with a sequence of increasingly
172 polar solvents; three times with dichloromethane (DCM), three times with

173 DCM/methanol (1:1, v/v) and two times with methanol. The total lipid extract was
174 then base hydrolyzed in 1M KOH/methanol (5% H₂O in volume) at 80°C for 2 h. The
175 solution was extracted at least 6 times with *n*-hexane, and the combined extracts were
176 dried under a stream of N₂ gas. Extracts were separated into a saturated hydrocarbon
177 and a polar fraction on a short silica gel column using *n*-hexane and methanol as
178 eluents, respectively. Half of the polar fraction was filtered through 0.45 µm PTFE
179 syringe filters and dried under nitrogen gas and used to analyze the GDGT
180 distribution.

181 The GDGTs were analyzed using an Agilent 1200 series liquid chromatography
182 and triple quadruple mass spectrometry (LC-MS²) system, equipped with an
183 autosampler and ChemStation manager software. Samples were spiked with an
184 internal C₄₆ GDGT standard (Huguet et al., 2006) and re-dissolved in 300µl
185 *n*-hexane/isopropanol (99:1, v/v). Samples (10µl) were injected and separation of
186 GDGTs, including 5-and 6-methyl brGDGTs, was achieved using two silica columns
187 in tandem (150 mm ×2.1 mm, 1.9 µm, Thermo Finnigan; USA) maintained at 40 °C.
188 EtOAc was used instead of the widely used isopropanol (IPA) as it has lower polarity,
189 leading to better separation of GDGT isomers. GDGTs eluted isocratically for the first
190 5 min with 84% A and 16% B, where A = *n*-hexane and B = EtOAc. The following
191 elution gradient was used: 84/16 A/B to 82/18 A/B from 5–65 min and then to 100%
192 B in 21 min, followed by 100% B for 4 min to wash the column and then back to
193 84/16 A/B to equilibrate the column for 30 min. We used a constant flow rate of 0.2
194 ml/min throughout. GDGTs were ionized in an atmospheric pressure chemical

195 ionization (APCI) chamber with single ion monitoring at m/z 1050, 1048, 1046, 1036,
196 1034, 1032, 1022, 1020 and 1018 for the brGDGTs and m/z 1292 for crenarchaeol.
197 The MS conditions followed Hopmans et al. (2000). GDGTs were quantified from
198 integrated peak areas of the $[M+H]^+$ ions. The relative response ratio of the GDGTs
199 relative to the internal C₄₆ GDGT standard was set at 1:1, allowing for
200 semi-quantitative concentrations.

201 In addition to new data from the Gushantun peat deposit, we also use GDGT data
202 (some previously published such as MAAT_{peat}) from the nearby Hani peat deposit. For
203 details on the age model and sample preparation, see Zheng et al. (2017).

204

205 *2.4. BrGDGT-based climate proxies*

206 For this study, the global peat-specific brGDGT calibrations of Naafs et al.
207 (2017a) were used to reconstruct mean annual air temperature (MAAT) and pH. The
208 standard (or root mean square) errors of the temperature and pH calibrations are 4.7
209 °C and 0.8, respectively. These proxies are based on the degree of methylation
210 (MBT_{5me'}) and cyclisation (CBT_{peat}) of brGDGTs and built on the original work done
211 using mineral soils (Weijers et al., 2007; De Jonge et al., 2014). Labeling of brGDGTs
212 follows the established protocols with Roman numbers indicating none (I), one (II) or
213 two (III) additional methyl groups at the C5 or C6 (') position and letters indicating
214 none (a), one (b), or two (c) cyclopentane moieties (See the supplementary file for the
215 structures; De Jonge et al., 2014; Naafs et al., 2017a):

216 (1) $MBT'_{5ME} = \frac{(Ia + Ib + Ic)}{(Ia + Ib + Ic + IIa + IIb + IIc + IIIa)}$

217

218 (2) $MAAT_{peat} = 52.18 \times MBT'_{5me} - 23.05 \quad (R^2 = 0.76, RMSE = 4.7 \text{ } ^\circ\text{C})$

219 (3) $CBT_{peat} = \log\left(\frac{Ib + IIa' + IIb + IIb' + IIIa'}{Ia + IIa + IIIa}\right)$

220 (4) $pH = 2.49 \times CBT_{peat} + 8.07 \quad (R^2 = 0.58, RMSE = 0.8)$

221 To reconstruct changes in the relative abundance of 5-methyl over 6-methyl
 222 brGDGTs, we used:

223 (5) IR_{6me}

224 $= \left(\frac{IIa' + IIb' + IIc' + IIIa' + IIIb' + IIIc'}{IIa + IIa' + IIb + IIb' + IIc + IIc' + IIIa + IIIa' + IIIb + IIIb' + IIIc + IIIc'} \right)$

225

226 (6) $f(6 - \text{Methyl brGDGTs})$

227 $= \frac{(IIa' + IIb' + IIc' + IIIa' + IIIb' + IIIc')}{(Ia + Ib + Ic + IIa + IIa' + IIb + IIb' + IIc + IIc' + IIIa + IIIa' + IIIb + IIIb' + IIIc + IIIc')}$

228

229 3. Results

230 The full suite of 15 brGDGTs was present in the Gushantun peat sequence.

231 5-methyl brGDGTs were more abundant than 6-methyl brGDGTs in all samples.

232 6-methyl brGDGTs were most abundant in the lacustrine section at the bottom of the

233 core. Generally brGDGT-Ia was the dominant brGDGT, but brGDGT-IIa and -IIIa

234 were also present in significant amounts. The cyclopentane-containing brGDGTs,

235 especially IIIb, IIIb', IIIc and IIIc', occurred in very low abundance or were not
236 detected. brGDGT IIa' was the most abundant of the 6-methyl brGDGTs, followed by
237 IIIa' and IIb'.

238 MBT_{5me'} and reconstructed mean annual air temperatures based on the global
239 peat-specific calibration (MAAT_{peat}) have been applied to the Hani peat and
240 previously published (Zheng et al., 2017). For Gushantun, values for the MBT_{5me'}
241 index ranged from 0.36 to 0.64, with a mean of 0.51. MAAT_{peat}-based temperatures
242 range from -4.2 to 10.2 ± 4.7 °C with a mean value of 3.4 °C (Fig. 3a). Temperatures
243 are higher during the early Holocene (about 11 to 6 cal kyr BP), with values between
244 3.1 and 10.2 ± 4.7 °C, and then decrease to values between 0.8 and 4.1 ± 4.7 °C
245 during the late Holocene. The lower MAAT_{peat} values during the late Holocene
246 correspond to higher fractional abundances of 5-methyl brGDGTs.

247 The CBT_{peat} index at Gushantun ranges from -1.52 to -0.12 with a mean of -0.79.
248 Reconstructed pH ranges from 4.3 to 7.8 ± 0.8 with a mean value of 6.1 and displays a
249 general decrease from the early Holocene to the late Holocene (Fig. 4c). The pH
250 values covary with the IR_{6me}, and the fractional abundances of 6-methyl brGDGTs
251 (Fig. 4a, b and c). The overall decrease in pH coincides with a general decrease in the
252 abundance of crenarchaeol (Fig. 5c and d). The CBT_{peat} and pH values vary from
253 -0.52 to -1.12 and 5.2 to 6.7 ± 0.8 , respectively, at Hani peat (Fig. 5b). Crenarchaeol
254 concentrations mostly range from and 0 to 73 ng/g at Hani (Fig. 5a).

255 **4. Discussion**

256 *4.1 Holocene temperature variations in the Gushantun peat core*

257 The global peat calibration of Naafs et al. (2017a) is predominantly based on
258 low-temperature peats from the regions between 40 °N and 60 °N, which covers the
259 latitude and temperature of our peat in Northeast China. Crucially, the MAAT_{peat} in
260 the top ~50 cm of Gushantun peat core (~3 to 7 °C with most values around 3 °C) fits
261 well with the observed instrumental yearly mean air temperature in the region of
262 between 3 and 7 °C from 1951 to 2013 and the modern-day MAAT of ~3 °C (Liu,
263 1989). As such this global peat calibration is well-suited to reconstruct temperature in
264 this region. Although care has to be taken to use the global peat-specific calibration to
265 reconstruct small-scale (1-2 °C) and brief (< 1 kyr) temperature anomalies (Naafs et
266 al., 2017a), here we apply the calibration across the last 13,000 years to determine
267 whether the several thousand years long period of the early Holocene is different from
268 the several thousand years long period of the late Holocene.

269 We do not have data from before 13 kyr BP, but the lowest temperatures around ca.
270 12.7 kyr BP could be related to the global cooling during the Younger Dryas. However,
271 we must emphasize that these sediments represent lacustrine rather than peat
272 deposition and changes in depositional environment almost certainly have an impact
273 on brGDGT-based temperature proxies (Sun et al., 2011; Peterse et al., 2012). For the
274 Holocene our mean annual air temperature reconstruction indicates a warm early
275 Holocene and a colder late Holocene climate (Fig. 3a). The reconstructed difference in
276 temperature between the late and early Holocene is around 5-7 °C, large enough to be
277 accurately captured by the MAAT_{peat} record. The observation that the highest

278 temperatures occurred during the early Holocene at Gushantun is consistent with other
279 records from China that indicate highest MAAT during the early Holocene (He et al.,
280 2004; Gao et al., 2012; Jia et al., 2013; Peterse et al., 2014; Zheng et al., 2017). The
281 degree of warming reconstructed using MAAT_{peat} at Gushantun during the early
282 Holocene (5-7 °C) is similar to that observed at the nearby Hani peat (6-7 °C) using
283 MAAT_{peat} (Fig. 3b) (Zheng et al., 2017). They are also consistent with the relatively
284 higher percentages of the thermophilous broadleaf trees, including *Quercus*, *Corylus*,
285 *Juglans* and *Ulmus*, during this interval in the same peat (e.g., Liu, 1989, Zhao et al.,
286 2015) and multiproxy based temperature reconstructions that indicate higher than
287 modern MAAT between 8 and 3 ka in NE China (Shi et al., 1994). Similarly, pollen
288 records from nearby Mount Changbai and Sihailongwan Maar lake (Fig. 3c) indicate
289 higher temperatures during the early Holocene compared to modern (He et al., 2004;
290 Stebich et al., 2015). Furthermore, MAAT records from the Chinese Loess Plateau
291 also suggested temperature maxima 7-9 °C higher than modern during the early
292 Holocene (Peterse et al., 2014; Gao et al., 2012; Jia et al., 2013). Consequently, we
293 consider the temperatures obtained using the global peat calibration to be
294 representative of climate in (NE) China.

295 The highest temperatures occurred between ca. 8 and 6.8 kyr BP, with occasional
296 annual mean temperatures $> 8.0 \pm 4.7$ °C, compared to the modern-day MAAT of
297 ~ 3 °C. These relatively high temperatures were interrupted by slightly lower values
298 between 10.5-10.2 kyr BP with temperatures ca. 5 ± 4.7 °C and between 8.7-8.3 kyr
299 BP with temperatures ca. 6 ± 4.7 °C. Although well within the calibration error of our

300 proxy, these two brief cool intervals could correspond with the ‘10.3 ka event’ and
301 ‘8.2 ka event’ recorded in climatic records from the North Atlantic (Bond et al., 2001).
302 From ca. 6 kyr BP, MAAT_{peat}-derived temperatures are colder with most values below
303 ~4 °C, and reconstructed temperatures for the last millennium are close to the
304 present-day mean annual air temperature in the region of ~3 °C.

305 The overall MAAT pattern at Gushantun peat – with a clear early Holocene
306 maximum and cold conditions during the mid- and late Holocene – is broadly
307 consistent with other climatic records from (NE) China. However, there are some
308 discrepancies in the trends recorded in the Gushantun and nearby Hani peats. The
309 Gushantun MAAT_{peat} record does not exhibit a cooling during the last 2 kyr and the
310 reconstructed temperature in the very top sample is ~7 °C. A potential seasonal bias at
311 the very top of the peat core may be responsible for the different trends, as has been
312 observed for some high-latitude peats due to intense summer warming (Naafs et al.,
313 2017a). Furthermore, small discrepancies in MAAT_{peat} between Gushantun and the
314 nearby Hani peat could be related to peat soil heterogeneity (Weijers et al., 2007),
315 difference in vegetation cover (Peterse et al., 2012), and water content (Dang et al.,
316 2016) that can affect the brGDGTs distributions. Despite the discrepancy, the absolute
317 MAAT estimates in the top ~ 50 cm are close to the present-day temperature in two
318 peats, providing confidence in our absolute MAAT estimates.

319 *4.2 Holocene moisture patterns in NE China, other Asian monsoon regions and arid*
320 *central Asia*

321 4.2.1 Holocene moisture variations in NE China

322 In addition to the temperature reconstructions, the Gushantun peat GDGT
323 distributions are characterized by changes in concentrations of crenarchaeol (Fig. 5d),
324 a biomarker specific to *Thaumarchaeota* (Sinninghe Damsté et al., 2002).
325 *Thaumarchaeota* generally account for the majority of the archaeal community in dry
326 soils (Timonen and Bomberg, 2009; Bates et al., 2011), but are generally less
327 proportionally abundant in peat, which also contains abundant *Euryarchaeota* as
328 methanogens (Zheng et al., 2015). Consequently, the relative abundance of
329 crenarchaeol tends to be relatively high in mineral soils (depending on temperature;
330 Xie et al., 2012; Yang et al., 2014), but low in peat (Pancost and Sinninghe Damsté,
331 2003; Zheng et al., 2015).

332 Therefore, we interpret the higher concentrations of crenarchaeol at Gushantun
333 during the early Holocene (> 5-6 ky BP) as evidence for drier conditions in this
334 peat-forming environment and interpret lower concentrations during the late Holocene
335 as indicative of wetter, more typical peat-forming conditions (Fig. 5d). This
336 interpretation is consistent with drying events in other peats also being associated with
337 increased crenarchaeol concentrations (Zheng et al., 2015). The nearby Hani peat core
338 exhibits some similar features in the crenarchaeol concentration profile, i.e. a
339 long-term (but irregular) decrease over the past 6 to 8 kyr. However, concentrations
340 are higher at Hani throughout the records, and there are strong differences in the
341 profiles prior to 8 kyr (Fig. 5a).

342 This appears to reflect differences in the thaumarchaeotal population between the

343 two peats, likely arising from hydrology and vegetation, and these differences might
344 have been greater during the early formation of the peat, i.e. from 8 to 10 kyr.
345 Crenarchaeol is more abundant in warm settings than in low temperature settings
346 (Schouten et al., 2000; Zhang et al., 2006), so the low absolute and relative
347 crenarchaeol abundances from the Hani peats between ca. 8-10 kyr BP are possibly
348 due to the lower temperature at Hani at this time (see Fig. 3b). So although in general
349 both peat cores indicate higher concentrations of crenarchaeol during the early
350 Holocene, which we interpret to reflect drier conditions, there is the need for further
351 investigation into crenarchaeol as an indicator of moisture in other peat settings from
352 around the world.

353 Further evidence for changes in wetland hydrology in NE China across the
354 Holocene comes from the brGDGT-reconstructed pH at both Hani and Gushantun,
355 with high values during the early Holocene and low pH during the late Holocene (Fig.
356 5b and c). This trend is the most obvious at Gushantun. In general, low effective
357 precipitation results in dry bog conditions, which suppresses the production of organic
358 acids (e.g., Clymo, 1984) and yields high pH values. This is in agreement with the
359 previous results from other peats where elevated pH values correspond to low
360 monsoon precipitation (a dry climate) (Zheng et al., 2015; Wang et al., 2017).
361 However, the pH values diverge between the two peats after ~4 kyr BP, increasing at
362 Hani and continuing to decrease at Gushantun. This discrepancy in the pH variations
363 between the two peats could be attributed to hydrological conditions and vegetation
364 changes. The Hani river and its tributaries go through Hani peatland, thereby affecting

365 the sedimentary environment and water content of Hani peatland, whereas Gushantun
366 peatland does not have such an influence. Additionally, the abundance of *Sphagnum*
367 vegetation decreases at Hani after 4 ky BP as *Betula*, *Potentilla*, and *Carex* become
368 more abundant (Schröder et al., 2007); the decrease in *Sphagnum* abundance could be
369 associated with an increase in pH (Gagnon et al., 1992). Thus, the dissimilarity in
370 small-scale pH variations during the (late) Holocene between the two peats might
371 result from different hydrological conditions, vegetation and the specific sediment
372 settings and features, although the same calibration and method have been used. This
373 does illustrate the complexity of peat as an archive of hydrological change and
374 dictates caution in our discussion of Holocene change.

375 More evidence for changes in the moisture content across the Holocene comes
376 from the high IR_{6me} values during the early Holocene (Fig. 4a). High IR_{6me} values
377 occur in mineral soils and peat characterized by (arid) alkaline conditions (De Jonge
378 et al., 2014; Dang et al., 2016; Naafs et al., 2017a). The higher IR_{6me} values during the
379 early Holocene provide complementary evidence for drier conditions during the early
380 Holocene. The highest values between 12 and 14 kyr BP likely reflect higher pH
381 values during the lake phase.

382 The conclusion that the Gushantun (and Hani) peat and surrounding region
383 became wetter through the Holocene (although note the complexity of the pH record
384 at Hani) is supported by the rise in conifer tree percentages such as *Pinus* (which grow
385 in humid settings (Sun et al., 1996)) from the same peatland and nearby lake
386 sediments (Liu et al., 1989; Zhao et al., 2015; Stebitch et al., 2015), as well as the

387 increase in effective precipitation across the Holocene indicated by the *n*-alkane C₂₇
388 δ D and *Paq* records at Hani (Seki et al., 2009; Zhou et al., 2010). Pollen-based mean
389 annual precipitation (*Pann*) estimates continuously increased from the early Holocene
390 and reached a maximum value around 4000 cal yr BP in Sihailongwan Maar lake
391 (Stebich et al., 2015; Fig. 6h); *Pann* variations do indicate that mean annual
392 precipitation decreased after 4 kyr BP (Fig. 6h), but it remained at a relatively high
393 level in comparison with that of the early Holocene (Stebich et al., 2015). Similarly,
394 Zhou et al. (2016) proposed that relatively higher pollen percentages of trees
395 including *Pinus* and *Betula* indicate wetter climate conditions during the mid- to late
396 Holocene (after 5 kyr BP) in Tianchi Lake compared to the early Holocene (Fig. 6g).
397 Thus, our results are consistent with other climate reconstructions from the region that
398 indicate an increase in effective precipitation from the early Holocene to late
399 Holocene in NE China (Liu et al., 1989; Zhou et al., 2010; Zhou et al., 2016; Stebich
400 et al., 2015), although the exact timing differs between different settings and records.
401 We also note that although many of these records are for annual precipitation, that is
402 today derived primarily from summer monsoon precipitation in NE China.

403

404 *4.2.2 Comparison of Holocene moisture patterns in NE China with East Asian* 405 *monsoon regions and arid central Asia*

406 Leaf wax (*n*-alkane) δ D values, GDGT distributions and pollen records, from a
407 combination of peats and lake sediments, all indicate a dry early Holocene and a

408 humid middle to late Holocene in NE China (Fig. 6g-i). However, this evolution
409 differs from that known from northern China, including EASM margin regions and
410 monsoonal eastern China (Liu et al., 2015). It is also opposite to that recorded by the
411 high-resolution stalagmite $\delta^{18}\text{O}$ records from northeast China, northern China and
412 Southern China (Fig. 6b; Wu et al., 2011; Cai et al., 2010; Tan, 2009; Dykoski et al.,
413 2005; Wang et al., 2005a) and the biomarker records from the Pearl River Estuary
414 (Strong et al., 2013). Liu et al. (2015) summarized pollen-based proxy evidence from
415 lake sediments, paleosol development, and other proxies from loess-paleosol
416 sequences and aeolian activity in the northern Chinese sandlands from various
417 geographical regions and concluded that the EASM precipitation maximum occurred
418 during the mid-Holocene (ca. 8-3 kyr BP).

419 Stalagmite $\delta^{18}\text{O}$ records from Dongge cave in southern China indicate an early
420 Holocene (ca. 10-5 kyr BP) EASM maximum (Fig. 6b; e.g., Dykoski et al., 2005;
421 Wang et al., 2005a). In particular, the Dongge Cave $\delta^{18}\text{O}$ record was originally
422 interpreted to record elevated monsoon precipitation (wet) between 10-6 kyr (An et al.,
423 2000). However, subsequent studies on moisture/precipitation from different sites
424 have challenged this conclusion and the record has been re-interpreted as indicating
425 maximum effective precipitation during the early/mid-Holocene in EASM regions
426 (Herzschuh et al., 2006; Wang et al., 2010; Zhao et al., 2009; Zhang et al., 2011; Chen
427 et al., 2015). More recently, Zhou et al. (2016) proposed that the Holocene Optimum,
428 defined as a period with high monsoon precipitation, began ca. 6 kyr BP in NE China,
429 although it is likely that a slightly northward transgression of the high monsoon

430 precipitation occurred (Zhou et al., 2016). Nonetheless these studies collectively
431 indicate that the Holocene moisture optimum occurred largely during the
432 early/mid-Holocene with effective moisture or monsoon precipitation decreasing
433 during the late Holocene in the EASM region. NE China is influenced by the East
434 Asian monsoon system and that seems to be manifested in some aspects of our
435 records (i.e. Hani peat pH) and other records (Pollen and Pann records from lakes; Fig.
436 6g and h) from 4 kyr. But the long-term decline in moisture over the past 8 kyr
437 recorded in EASM-dominated regions is not seen in most records and it appears that
438 other climatic factors have influenced the moisture history of NE China (Fig. 6).

439 A regional synthesis from the North Xinjiang area based on fifteen published
440 climate proxy records also indicates a persistent increase towards wetter conditions
441 from the early Holocene to late Holocene, similar to our findings (Fig. 6k; Wang et al.,
442 2013). Recently, four well-dated Holocene loess-paleosol sequences from the northern
443 slopes of the Tianshan Mountains and the Yili River valley of Xinjiang, located in the
444 core area of arid central Asia, also indicated increasing moisture in the region from
445 about 8 kyr BP (Fig. 6j) (Chen et al., 2016). These moisture records from central Asia
446 are consistent with our findings from NE China (Fig. 6g-k), but differ significantly
447 from the trends of EASM evolution during the Holocene (Fig. 1 and Fig. 6b-d).

448 In addition, the MAAT_{peat} record from Gushantun and Hani indicate highest
449 temperatures from 11-6 kyr BP, which broadly corresponds with a period of relatively
450 warm climate in the middle and high latitudes of the Northern Hemisphere, including
451 the classical ‘Holocene Optimum’ defined by high monsoon precipitation in both

452 northern and southern China (e.g., Zhou et al., 2007; Zhao et al., 2009; Ran et al.,
453 2013). Thus, it appears that the thermal maximum during the early Holocene
454 corresponds to low effective precipitation in NE China but high effective precipitation
455 in other EASM-influenced regions: i.e. the temperature-moisture patterns in NE China
456 were mainly dominated by warm-dry, cold-wet episodes during the Holocene. This is
457 similar to climate relationships in the core area of arid central Asia that also exhibit a
458 transition from a warm-dry early Holocene to cold-wet late Holocene (Huang et al.,
459 2009; Jiang et al., 2013); but it is clearly different from other East Asian monsoon
460 regions including South China and North China which show warm-wet and cold –dry
461 climate Holocene patterns (e.g., Wang et al., 2005a).

462

463 *4.3 Possible forcing mechanisms of Holocene climate evolution in NE China*

464 The Western Pacific Subtropical High (WPSH) is the most important component
465 of the EASM and governs modern summer precipitation in NE China (Chu et al.,
466 2014). Considering the linkage between SSTs in the subtropical west Pacific and the
467 WPSH (Chu et al., 2014), we propose that increasing SST in the northern East China
468 Sea and Sea of Japan during the early Holocene (Ishiwatari et al., 2001; Kubota et al.,
469 2015) induced a northward shift of the WPSH. Consequently, the monsoon
470 precipitation band extended into NE China and increased rainfall in NE China. As
471 SSTs decreased during the late Holocene, the WPSH would have shifted southwards,
472 weakening its influence in NE China and presumably leading to a decrease in

473 precipitation in this region. However, our results (and those of others) indicate the
474 opposite – an increase in effective precipitation from the early Holocene to late
475 Holocene in NE China. Thus, the EASM precipitation driven by summer insolation
476 might not solely control Holocene moisture variations (from dry to wet) in NE China
477 (Fig. 6a-d and g-i). In particular, this partial discrepancy between NE China climate
478 relationships with other Asian monsoon regions implies the influence of additional
479 forcing mechanisms, as well as a possible link between NE China and the core area of
480 arid central Asia. Previous research attributed this difference to local SST changes in
481 the Sea of Japan (Zhou et al., 2010): high SSTs in the Sea of Japan during the early
482 Holocene could have amplified the evaporation rate, resulting in the drier climate
483 conditions. Lower SSTs and the cold climate (low MAAT) during the mid- and late
484 Holocene caused less evaporation, resulting in wet climate conditions. Although the
485 relatively dry climate in NE China could be partly attributed to enhanced evaporation
486 related to the additional warming caused by higher SST from the Sea of Japan (Zhou
487 et al., 2010), less evaporation and decreased EASM precipitation seems insufficient to
488 explain the increasingly wet conditions during the late Holocene. Nor can wetter
489 conditions be explained by strengthening of the East Asian winter monsoon (EAWM)
490 during the late Holocene, as it carries a relatively dry air mass to NE China (Zhang et
491 al., 2016).

492 The temperature-moisture evolution patterns in NE China, however, are
493 coincident with those observed in the core area of arid central Asia; these also exhibit
494 a transition from a warm-dry early Holocene to cold-wet late Holocene (Huang et al.,

495 2009; Jiang et al., 2013; Chen et al., 2016). These relationships are also observed in
496 the mid-latitudes of Europe between ca. 50°N and 43°N during the Holocene (Magny
497 et al., 2003). These evidently resulted from variations in the strength of the Westerly
498 jet, in turn related to the thermal gradient between high and low latitudes. Similarly,
499 increased Holocene moisture/precipitation in the core area of the arid central Asia has
500 been attributed to an increase in the strength of the westerlies (Chen et al., 2016).
501 Thus, this suggests that the westerlies might be a major link between NE China, the
502 core area of arid central Asia and mid-latitude Europe, as we have also suggested
503 based on enhanced MAAT variability recorded in the Hani peat (Zheng et al., 2017).
504 Indeed, the strength of the westerlies, inferred from the insolation gradient between
505 35°N and 55°N, could have gradually increased since the early Holocene (Rossby et
506 al., 1939; Chen et al., 2016). In this scenario, increasing winter insolation caused an
507 increase in winter temperature from the early Holocene to the late Holocene in
508 Northern Europe (Fig. 6e; Davis et al., 2003), leading to enhanced water vapor
509 evaporation over the Mediterranean, Black and Caspian Seas. Previous research has
510 confirmed that this air with elevated water vapor contents could have been delivered
511 by strengthened mid-latitude westerlies to the Xinjiang region (Northern China) in the
512 core area of arid central Asia (Fig. 6f; Zhang et al., 2016; Chen et al., 2016; Long et
513 al., 2017). In fact, the westerlies could have penetrated even further eastward
514 (Vandenberghe et al., 2006), even to Japan (Yamada, 2004). Therefore, both higher
515 water vapor contents and strengthened westerly winds could have brought more
516 moisture to NE China, thereby causing wetter conditions, during the late Holocene

517 (Fig. 6f).

518 In addition, changes in Arctic sea ice extent and shifts in the position of the
519 Okhotsk High also play an important role in regulating climate (including moisture) in
520 NE China (e.g., Guo et al., 2014; Chu et al., 2014). According to Guo et al. (2014),
521 lower spring Arctic sea ice extent is associated with less rainfall in the Northern
522 EASM region, and vice versa. Consistent with this scenario, the relative abundance of
523 sea ice-related diatoms from the West Okhotsk Sea shows a long-term increase
524 through the Holocene (Harada et al., 2014). Thus, increased sea ice extent during the
525 late Holocene could have caused high precipitation in NE China in comparison with
526 the early Holocene. Furthermore, decreasing SST in the Okhotsk Sea from the early
527 Holocene to late Holocene could have strengthened the Okhotsk high that brings
528 moisture into the Far East including NE China (Kakei and Sekine, 2004; Harada et al.,
529 2014). Clearly, our records cannot unravel these complex and multiple climatic
530 controls on rainfall and peat water balance. They do, however, clearly indicate a
531 decoupling between NE China and other EASM-dominated regions that requires
532 further critical analysis and could have implications for our understanding of how the
533 EASM evolves in the future.

534

535 **5. Conclusions**

536 In this study we present a detailed GDGT data set covering the last 13,000 years
537 from a peat sequence in the Changbai Mountain in NE China. The brGDGT-based

538 temperature reconstruction from Gushantun peat indicates that mean annual air
539 temperatures in NE China during the early Holocene were 5-7 °C higher than today. A
540 constantly high air temperature is reconstructed between ca. 8 and 6.8 kyr BP, with
541 maximum annual mean temperatures exceeding ca. 8.0 °C. Lower temperatures are
542 recorded from around ca. 6 kyr BP onwards, with most values $< 4 \pm 4.7$ °C.
543 Crenarchaeol concentrations, brGDGT-based pH values, and relative abundance of
544 6-methyl brGDGTs obtained from both the Gushantun and nearby Hani peat generally
545 indicate that peat soil moisture, and by inference effective precipitation, increased
546 from the early Holocene to the late Holocene in NE China. Therefore, the
547 temperature-moisture patterns in NE China appear to be dominated by warm-dry and
548 cold-wet alternations during the Holocene, which is largely consistent with other data
549 from NE China. Comparisons with other proxy records from the EASM regions reveal
550 that the reconstructed climate development differs from the Holocene moisture
551 evolution in Southern/Eastern China and Northern China, but is consistent with the
552 core area of Arid Central Asia such as Xinjiang. We suggest that changes in i) the
553 intensity of the mid-latitude westerlies associated with winter insolation and EASM, ii)
554 SST-modulated evaporation in the Japan Sea, iii) Arctic sea ice extent and iv) the shift
555 of the Okhotsk High all could have played an important role in the out-of-phase
556 relationship in the moisture evolution between NE China and other EASM regions
557 and in the strong climatic similarities between NE China and the core area of arid
558 central Asia during the Holocene.

559

560 **Acknowledgements**

561 This work was supported by National Natural Science Foundation of China Grants
562 (41372033, 41072024), Outstanding Youth Foundation of Shaanxi Province, a Marie
563 Curie International Incoming Fellowship within the 7th European Community
564 Framework Programme, the fund from State Key Laboratory of Loess and Quaternary
565 Geology (SKLLQG1731) and MOST Special Fund from the State Key Laboratory of
566 Continental Dynamics, Northwest University. R.D. Pancost and B.D.A. Naafs were
567 funded through the advanced ERC grant “the greenhouse earth system” (T-GRES,
568 project reference 340923). We thank the editor, Phil Meyers and 2 anonymous
569 reviewers for valuable comments.

570

571 **References**

- 572 An, Z.S., Colman, S.M., Zhou, W.J., Li, X.Q., Brown, E.T., Jull, A.J.T., Cai, Y.J.,
573 Huang, Y.S., Lu, X.F., Chang, H., Song, Y.G., Sun, Y.B., Xu, H., Liu, W.G., Jin,
574 Z.D., Liu, X.D., Cheng, P., Liu, Y., Ai, L., Li, X.Z., Liu, X.J., Yan, L.B., Shi,
575 Z.G., Wang, X.L., Wu, F., Qiang, X.K., Dong, J.B., Lu, F.Y., Xu, X.W., 2012.
576 Interplay between the Westerlies and Asian monsoon recorded in Lake Qinghai
577 sediments since 32 ka. *Sci. Rep.* 2, 619; DOI:10.1038/srep00619.
- 578 An, Z.S., Porter, S.C., Kutzbach, J.E., Wu, X.H., Wang, S.M., Liu, X.D., Zhou, W.J.,
579 2000. Asynchronous Holocene optimum of the East Asian monsoon. *Quat. Sci.*
580 *Rev.* 19,743–762.
- 581 Barber, K.E., Maddy, D., Rose, N., Stevenson, A.C., Stoneman, R.E., Thompson, R.,

582 2000. Replicated proxy-climate signals over the last 2000 years from two
583 distant peat bogs: new evidence for regional palaeoclimate teleconnections.
584 *Quat. Sci. Rev.* 19, 481–487.

585 Barber, Keith E., Chambers, Frank M. and Maddy, D., 2003. Holocene palaeoclimates
586 from peat stratigraphy: macrofossil proxy-climate records from three oceanic
587 raised peat bogs in England and Ireland. *Quat. Sci. Rev.* 22, 521–539.

588 Bates, S.T., Berg-Lyons, D., Caporaso, J. G., Walters, W. A., Knight, R., Fierer, N.,
589 2011. Examining the global distribution of dominant archaeal populations in soil.
590 *ISME J.* 5, 908–917.

591 Berger, A., Loutre, M.F., 1991. Insolation values for the climate of the last 10 million
592 years. *Quat. Sci. Rev.* 10, 297–317.

593 Blaauw, M. and Christen, J.A., 2011. Flexible paleoclimate age-depth models using
594 an autoregressive gamma process: Bayesian Analysis, 6, 457–474.

595 Bond, G., Kromer, B., Beer, J., Muscheher, R., Evans, M.N., Showers, W., Hoffmann,
596 S., Lotti-Bond, R., Hajdas, I., Bonani, G., 2001. Persistent solar influence on
597 North Atlantic climate during the Holocene. *Science*, 29, 2130–2136.

598 Cai, Y.J., Tan, L.C., Cheng, H., An, Z.S., Edwards, R.L., Kelly, M.J., Kong,
599 X.G., Wang, X.F., 2010. The variation of summer monsoon precipitation in central
600 China since the last deglaciation. *Earth Planet. Sci. Lett.* 291, 21–31.

601 Chen, F.H., Xu, Q.H., Chen, J.H., Birks, H.J.B., Liu, J.B., Zhang, S.R., Jin, L.Y., An,
602 C.B., Telford, R.J., Cao, X.Y., Wang, Z.L., Zahng, X.J., Selvaraj, K., Lü, H.Y.,
603 Li, Y.C., Zheng, Z., Wang, H.P., Zhou, A.F., Dong, G.H., Zhang, J.W., Huang,

604 X.Z., Bloemendal, J., Rao, Z.G., 2015. East Asian summer monsoon
605 precipitation variability since the last deglaciation. *Sci. Rep.*
606 <http://dx.doi.org/10.1038/srep11186>.

607 Chen, F.H., Jia, J., Chen, J.H., Li, G.Q., Zhang, X.J., Xie, H.C., Xie, D.S., Huang, W.,
608 An, C.B., 2016. A persistent Holocene wetting trend in arid central Asia, with
609 wettest conditions in the late Holocene, revealed by multi-proxy analyses of
610 loess-paleosol sequences in Xinjiang, China. *Quat. Sci. Rev.* 146, 134–146.

611 Cheng, B., Chen, F., Zhang, J., 2013. Palaeovegetational and palaeoenvironmental
612 changes since the last deglacial in Gonghe Basin, northeast Tibetan Plateau. *J.*
613 *Geogr. Sci.* 23, 136–146.

614 Chu, G., Sun, Q., Xie, M., Lin, Y., Shang, W., Zhu, Q., Shan, Y., Xu, D., Rioual, P.,
615 Wang, L., Liu, J., 2014. Holocene cyclic climatic variations and the role of the
616 Pacific Ocean as recorded in varved sediments from northeastern China. *Quat.*
617 *Sci. Rev.* 15, 85–95.

618 Clymo, R.S., 1984. Sphagnum-dominated peat bog: a naturally acid ecosystem.
619 *Proceedings of the Royal Society of London*, 305, 487–499.

620 Dang, X., Yang, H., Naafs, B.D.A., Pancost, R.D., Evershed, R.P., Xie, S., 2016. Direct
621 evidence of moisture control on the methylation of branched glycerol dialkyl
622 glycerol tetraethers in semi-arid and arid soils. *Geochim. Cosmochim. Acta* 189,
623 24–36, doi: 10.1016/j.gca.2016.06.004.

624 Davis, B.A.S., Brewer, S., Stevenson, A.C., Guiot, J., Data contributors, 2003. The
625 temperature of Europe during the Holocene reconstructed from pollen data. *Quat.*

626 Sci. Rev. 22, 1701–1716.

627 De Jonge, C., Hopmans, E.C., Stadnitskaia, A., Rijpstra, W.I.C., Hofland, R., Tegelaar,
628 E., Sinninghe Damsté, J.S., 2013. Identification of novel penta- and
629 hexamethylated branched glycerol dialkyl glycerol tetraethers in peat using HPLC–
630 MS², GC–MS and GC–SMB-MS. *Org. Geochem.* 54, 78–82, doi:
631 10.1016/j.orggeochem.2012.10.004.

632 De Jonge, C., Hopmans, E.C., Zell, C.I., Kim, J.-H., Schouten, S., Sinninghe Damsté,
633 J.S., 2014. Occurrence and abundance of 6-methyl branched glycerol dialkyl
634 glycerol tetraethers in soils: implications for palaeoclimate reconstruction.
635 *Geochim. Cosmochim. Acta* 141, 97–112.

636 Dykoski, C.A., Edwards, R.L., Cheng, H., Yuan, D.X., Cai, Y.J., Zhang, M.L., Lin,
637 Y.S., Qing, J.M., An, Z.S., Revenaugh, J., 2005. A high-resolution absolute-dated
638 Holocene and deglacial Asian monsoon record from Dongge Cave, China. *Earth
639 Planet. Sci. Lett.* 233, 71–86.

640 Gagnon, Z.E., Glime, J.M., 1992. The pH-lowering ability of *Sphagnum magellanicum*
641 *Brid. J. Bryol.* 17, 47–57.

642 Gao, L., Nie, J.S., Clemens, S., Liu, W.G., Sun, J.M., Zech, R. and Huang, Y.S., 2012,
643 The importance of solar insolation on the temperature variations for the past 110
644 kyr on the Chinese Loess Plateau. *Palaeogeogr. Palaeoclimatol. Palaeoecol.* 317–
645 318, 128–133.

646 Guo, D., Gao, Y., Bethke, I., Gong, D., Johannessen, O.M., Wang, H., 2014.
647 Mechanism on how the spring Arctic sea ice impacts the East Asian summer

648 monsoon. *Theor. Appl. Climatol.* 115, 107–119.

649 Harada, N., Katsuki, K., Nakagawa, M., Matsumoto, A., Seki, O., Addison, J.A.,
650 Finney, B.P., Sato, M., 2014. Holocene sea surface temperature and sea ice
651 extent in the Okhotsk and Bering Seas. *Prog. Oceanogr.* 126, 242–253.

652 He, Y., Theakstone, W.H., Zhang, Z., Zhang, D., Yao, T., Chen, T., Shen, Y., Pang,
653 H., 2004. Asynchronous Holocene climatic change across China. *Quaternary Res.*
654 61, 52–63.

655 Herzschuh, U., 2006. Palaeo-moisture evolution in monsoonal Central Asia during the
656 last 50,000 years. *Quat. Sci. Rev.* 25, 163–178.

657 Hong, Y.T., Hong, B., Lin, Q.H., Shibata, Y., Hirota, M., Uchida, M., Zhu, Y.X.,
658 Leng, X.T., Wang, Y., Wang, H., Yi, L., 2005. Inverse phase oscillations
659 between the East Asian and Indian Ocean summer monsoons during the last
660 12000 years and paleo-El Niño. *Earth Planet. Sci. Lett.* 231, 337–346.

661 Hong, B., Liu, C.Q., Lin, Q.H., Yasuyuki, S., Leng, X.T., Wang, Y., Zhu, Y.X., Hong,
662 Y.T., 2009. Temperature evolution from the $\delta^{18}\text{O}$ record of Hani peat, Northeast
663 China, in the last 14000 years. *Sci. China Earth Sci.* 52, 952–964.

664 Hopmans, E.C., Schouten, S., Pancost, R.D., van der Meer, M.T.J. and Sinninghe
665 Damsté, J.S., 2000. Analysis of intact tetraether lipids in archaeal cell material and
666 sediments by high performance liquid chromatography/atmospheric pressure
667 chemical ionization mass spectrometry. *Rapid Commun. Mass Sp.* 14, 585–589.

668 Huang, X.Z., Chen, F.H., Fan, Y.X., Yang, M.L., 2009. Dry late-glacial and early
669 Holocene climate in arid Central Asia indicated by lithological and palynological

670 evidence from Bosten Lake, China. *Quat. Int.* 194, 19–27.

671 Huguet C., Hopmans E. C., Febo-Ayala W., Thompson D. H., Sinninghe Damste' J.
672 S. and Schouten S., 2006. An improved method to determine the absolute
673 abundance of glycerol dibiphytanyl glycerol tetraether lipids. *Org. Geochem.* 37,
674 1036–1041.

675 Ishiwatari, R., Houtatsu, M., Okada, H., 2001. Alkenone-sea surface temperature in
676 the Japan Sea over the past 36 kyr: warm temperatures at the last glacial
677 maximum. *Org. Geochem.* 32, 57–67.

678 Ise, T., Dunn, A.L., Wofsy, S.C., Moorcraft, P.R., 2008. High sensitivity of peat
679 decomposition to climate change through water-table feedback. *Nature Geosci.* 1,
680 763–766.

681 Kakei, M., Sekine, Y., 2004. Influence of sea surface temperature (SST) of the
682 Okhotsk Sea on the summer temperature in Hokkaido and Tohoku districts. *Mon.*
683 *Kaiyo* 36, 299–304.

684 Kubota, Y., Tada, R., Kimoto, K., 2015. Changes in East Asian summer monsoon
685 precipitation during the Holocene deduced from a freshwater flux reconstruction
686 of the Changjiang (Yangtze River) based on the oxygen isotope mass balance in
687 the northern East China Sea. *Clim. Past.* 11, 265–281.

688 Jia, G., Rao, Z., Zhang, J., Li, Z., Chen, F., 2013. Tetraether biomarker records from a
689 loess-paleosol sequence in the western Chinese Loess Plateau. *Front. Microbiol.*
690 4:199. doi: 10.3389/ fmicb.2013.00199

691 Jiang, Q.F., Ji, J.F., Shen, J., Matsumoto, R.Y.O., Tong, G.B., Qian, P., Ren, X.M.,

692 Yan, D.Z., 2013. Holocene vegetational and climatic variation in westerly –
693 dominated areas of Central Asia inferred from the Sayram Lake in northern
694 Xinjiang, China. *Sci. China Earth Sci.* 56, 339–353.

695 Jiang, W., Guo, Z., Sun, X., Wu, H., Chu, G., Yuan, B., Hatté, C., Guiot, J., 2006.
696 Reconstruction of climate and vegetation changes of Lake Bayanchagan (Inner
697 Mongolia): Holocene variability of the East Asian monsoon. *Quat. Res.* 65, 411–
698 420.

699 Li, N.N., Chambers, F.M., Yang, J.X., Jie, D.M., Liu, L.D., Liu, H.Y., Gao, G.Z., Gao,
700 Z., Li, D.H., Shi, J.C., Feng, Y.Y., Qiao, Z.H., 2017. Records of East Asian
701 monsoon activities in Northeastern China since 15.6ka, based on grain size
702 analysis of peaty sediments in the Changbai Mountains. *Quat. Int.* 447, 158–169.

703 Liu, J., 1989. Vegetational and climatic changes at Gushantun Bog in Jilin, NE China
704 Since 13,000 yr B.P. *Acta Palaeontol. Sin.* 28, 495–509 (in Chinese).

705 Liu, X.Q., Herzs Schuh, U., Shen, J., Jiang, Q.F., Xiao, X.Y., 2008. Holocene
706 environmental and climatic changes inferred from Wulungu Lake in northern
707 Xinjiang, China. *Quat. Res.* 70, 412–425.

708 Liu, Q., Li, Q., Wang, L., Chu, G., 2010. Stable carbon isotope record of bulk organic
709 matter from a sediment core at Moon Lake in the middle part of the Daxing’an
710 Mountain range, Northeast China during the last 21ka. *Quat. Sci.* 30, 1069–1077.

711 Liu, J.B., Chen, J.H., Zhang, X.J., Li, Y., Chen, F.H., 2015. Holocene East Asian
712 summer monsoon records in northern China and their inconsistency with Chinese
713 stalagmites $\delta^{18}\text{O}$ records. *Earth Sci. Rev.* 148, 194–208.

714 Long, H., Shen, J., Tsukamoto, S., Yang, L.H., Cheng, H.Y., Frechen, M., 2017.
715 Holocene moisture variations over the arid central Asia revealed by a
716 comprehensive sand-dune record th central Tian Shan, NW China. *Quat. Sci.*
717 *Rev.*174, 13–32.

718 Lu, H., Yi, S., Liu, Z., Mason, J.A., Jiang, D., Cheng, J., Stevens, T., Xu, Z., Zhang,
719 E., Jin, L., Zhang, Z., Guo, Z., Wang, Y., Otto-Bliesner, B., 2013. Variation of
720 East Asian monsoon precipitation during the past 21 k.y. and potential CO₂
721 forcing. *Geology* 41, 1023–1026.

722 Magny, M., Bégeot, C., Guiot, J., Peyron, O., 2003. Contrasting patterns of
723 hydrological changes in Europe in response to Holocene climate cooling phases.
724 *Quat. Sci. Rev.* 22,1589–1596.

725 Naafs, B.D.A., Inglis, G.N., Zheng, Y., Amesbury, M.J., Biester, H., Bindler, R.,
726 Blewett, J., et al., 2017a. Introducing global peat-specific temperature and pH
727 calibrations based on brGDGT bacterial lipids. *Geochim. Cosmochim. Acta* 208,
728 285–301, doi: 10.1016/j.gca.2017.01.038.

729 Naafs, B.D.A., Gallego-Sala, A.V., Inglis, G.N., Pancost, R.D., 2017b. Refining the
730 global branched glycerol dialkyl glycerol tetraether (brGDGT) soil temperature
731 calibration. *Org. Geochem.* 106, 48–56.

732 Peterse, F., van der Meer, J., Schouten, S., Weijers, J.W.H., Fierer, N., Jackson, R.B.,
733 Kim, J.-H., Sinninghe Damsté, J.S., 2012. Revised calibration of the MBT-CBT
734 paleotemperature proxy based on branched tetraether membrane lipids in surface
735 soils. *Geochim. Cosmochim. Acta* 96, 215–229.

- 736 Ran, M., Feng, Z., 2013. Holocene moisture variations across China and driving
737 mechanisms: a synthesis of climatic records. *Quat. Int.* 313–314, 179–193.
- 738 Reimer, P.J., Bard, E., Bayliss, a., Beck, J.W., Blackwell, P.W., Ramsey, C.B., Buck,
739 C.E., Cheng, H., Edwards, R.L., Friedrich, M., Grootes, P.M., Guilderson, T.P.,
740 Haflidason, H., Hajdas, I., Hatté, C., Heaton, T.J., Hoffmann, D.L., Hogg, A.G.,
741 Hughen, K.A., Kaiser, K.F., Kromer, B., Manning, S., Niu, M., Reimer, R.W.,
742 Richards, D.A., Scott, E.M., Southon, J.R., Staff, R.A., Turney, C.S.M., van der
743 Plicht, J., 2013. IntCal13 and Marine13 radiocarbon age calibration curves 0-
744 50,000 yr cal BP. *Radiocarbon* 55, 1869–1887.
- 745 Rossby, C.-G., Collaborators, 1939. Relationship between variations in the intensity
746 of the zonal circulation of the atmosphere and the displacements of
747 semipermanent centers of action. *J. Mar. Res.* 2, 38–55.
- 748 Shen, J., Liu, X.Q., Wang, S.M., Ryo, M., 2005. Palaeoclimatic changes in the
749 Qinghai Lake area during the last 18,000 years. *Quat. Int.* 136, 131–140.
- 750 Schouten, S., Hopmans, E.C., Pancost, R.D., Sinninghe Damsté, J.S., 2000.
751 Widespread occurrence of structurally diverse tetraether membrane lipids:
752 Evidence for the ubiquitous presence of low-temperature relatives of
753 hyperthermophiles. *PNAS* 97, 14421–14426, doi: 10.1073/pnas.97.26.14421.
- 754 Schouten, S., Hopmans, E.C., Sinninghe Damsté, J.S., 2013. The organic
755 geochemistry of glycerol dialkyl glycerol tetraether lipids: A review. *Org.*
756 *Geochem.* 54, 19–61, doi: 10.1016/j.orggeochem.2012.09.006.
- 757 Schröder, C., Thiele, A., Wang, S., Bu, Z., Joosten, H., 2007. Hani mire — a

758 percolation mire in northeast China. *Peatl. Int.* 2, 21–24.

759 Seki, O., Meyers, P.A., Kawamura, K., Zheng, Y., Zhou, W., 2009. Hydrogen isotopic
760 ratios of plant wax n-alkanes in a peat bog deposited in northeast China during
761 the last 16 kyr. *Org. Geochem.* 40, 671–677.

762 Shi, Y.F., Kong, Z.C., Wang, S.M., Tang, L.Y., Wang, F.B., Yao, T.D., Zhao, X.T.,
763 Zhang, P.Y., Shi, S.H., 1994. Climates and Environments of the Holocene
764 Megathermal Maximum in China, *Sci. China Chem.* 37, 481–493.

765 Sinninghe Damsté, J.S., Hopmans, E.C., Pancost, R.D., Schouten, S., Geenevasen,
766 J.A.J., 2000. Newly discovered non-isoprenoid glycerol dialkyl glycerol
767 tetraether lipids in sediments. *Chem. Commun.* 1683–1684.

768 Sinninghe Damsté, J.S., Schouten, S., Hopmans, E.C., van Duin, A.C.T., Geenevasen,
769 J.A.J., 2002. Crenarchaeol: the characteristic core glycerol dibiphytanyl glycerol
770 tetraether membrane lipid of cosmopolitan pelagic crenarchaeota. *J. Lipid Res.* 43,
771 1641–1651.

772 Slota, P.J., Jull, A.J.T., Linick, T.W., Toolin, L.J., 1987. Preparation of small samples
773 for ¹⁴C accelerator targets by catalytic reduction of CO₂. *Radiocarbon* 29, 303–
774 306.

775 Stebich, M., Rehfeld, K., Schlütz, F., Tarasov, P.E., Liu, J.Q., Mingram, J., 2015.
776 Holocene vegetation and climate dynamics of NE China based on the pollen
777 record from Sihailongwan Maar lake. *Quat. Sci. Rev.* 124, 275–289.

778 Stevens, T., Lu, H., Thomas, D.S., Armitage, S.J., 2008. Optical dating of abrupt
779 shifts in the late Pleistocene East Asian monsoon. *Geology* 36, 415–418.

780 Strong, D., Flecker, R., Valdes, P.J., Wilkinson, I.P., Rees, J.G., Michaelides, K.,
781 Zong, Y.Q., Lloyd, J.M., Yu, F.L., Pancost, R.D., 2013. A new regional,
782 mid-Holocene palaeoprecipitation signal of the Asian Summer Monsoon. *Quat.*
783 *Sci. Rev.* 78, 65–76.

784 Stuiver, M. and Reimer, P. J., 1993. Extended ¹⁴C database and revised CALIB
785 radiocarbon calibration program: *Radiocarbon* 35, 215–230.

786 Sun, X., Wang, F., Song, C., 1996. Pollen-climate response surfaces of selected taxa
787 from Northern China. *Sci. China, Ser. D* 39, 486–493.

788 Sun Q., Chu G., Liu M., Xie M., Li S., Ling Y., Wang X., Shi L., Jia G. and Lü H.,
789 2011. Distributions and temperature dependence of branched glycerol dialkyl
790 glycerol tetraethers in recent lacustrine sediments from China and Nepal. *J.*
791 *Geophys. Res.* 116, G01008.

792 Tan, M., 2009. Circulation effect: climatic significance of the short term variability of
793 the oxygen isotopes in stalagmites from monsoonal China—dialogue between
794 paleoclimate records and modern climate research. *Quat. Sci.* 29, 851–862 (in
795 Chinese, with English abstract).

796 Tao, S.C., An, C.B., Chen, F.H., Tang, L.Y., Wang, Z.L., Lu, Y.B., Li, Z.F., Zheng,
797 T.M., Zhao, J.J., 2010. Pollen-inferred vegetation and environmental changes
798 since 16.7 ka BP at Balikun Lake, Xinjiang. *Chinese Sci. Bull.* 55, 2449–2457.

799 Timonen, S., Bomberg, M., 2009. Archaea in dry soil environments. *Phytochem. Rev.*
800 8, 505–518.

801 Vandenberghe, J., Renssen, H., Huissteden, K., Nugteren, G., Konert, M., Lu, H.Y.,

802 Dodonov, A., Buylaert, J-P., 2006. Penetration of Atlantic westerly winds into
803 Central and East Asia. *Quat. Sci. Rev.* 25, 2380–2389.

804 Wang, Y., Cheng, H., Edwards, R.L., He, Y., Kong, X., An, Z., Wu, J., Kelly, M.J.,
805 Dykoski, C.A., Li, X., 2005a. The Holocene Asian monsoon: links to solar
806 changes and North Atlantic climate. *Science* 308, 854–857.

807 Wang, P.X., Clemens, S., Beaufort, L., Braconnot, P., Ganssen, G., Jian, Z.M.,
808 Kershaw, P., Sarnthein, M., 2005b. Evolution and variability of the Asian
809 monsoon system: state of the art and outstanding issues. *Quat. Sci. Rev.* 24, 595–
810 629.

811 Wang, S., Lü, H., Liu, J., Negendank, J.F.W., 2007. The early Holocene optimum
812 in-ferred from a high-resolution pollen record of Huguangyan Maar Lake in
813 south-ern China. *Chin. Sci. Bull.* 52, 2829–2836.

814 Wang, Y.J., Cheng, H., Edwards, R.L., Kong, X.G., Shao, X.H., Chen, S.T., Wu, J.Y.,
815 Jiang, X.Y., Wang, X.F., An, Z.S., 2008. Millennial- and orbital-scale changes in
816 the East Asian monsoon over the past 224,000 years. *Nature* 451, 1090–1093.

817 Wang, Y.B., Liu, X.Q., Herzschuh, U., 2010. Asynchronous evolution of the Indian
818 and East Asian Summer Monsoon indicated by Holocene moisture patterns in
819 monsoonal central Asia. *Earth Sci. Rev.* 103, 135–153.

820 Wang, W., Feng, Z., Ran, M., Zhang, C., 2013. Holocene climate and vegetation
821 changes inferred from pollen records of Lake Aibi, northern Xinjiang, China: a
822 potential contribution to understanding of Holocene climate pattern in
823 East-central Asia. *Quat. Int.* 311, 54–62.

- 824 Wang, W., Feng, Z.D., 2013. Holocene moisture evolution across the Mongolian
825 Plateau and its surrounding areas: a synthesis of climatic records. *Earth Sci. Rev.*
826 122, 38–57.
- 827 Wang, H.Y., Dong, H.L., Zhang, C.L., Jiang, H.C., Zhao, M.X., Liu, Z.H., Lai, Z.P.,
828 Liu, W.G., 2014. Water depth affecting thaumarchaeol production in lake Qinghai,
829 northeastern Qinghai-Tibetan plateau: Implications for paleo lake levels and
830 paleoclimate. *Chem. Geol.* 368, 76–84.
- 831 Wang, M., Zheng, Z., Man, M., Hu, J., Gao, Q., 2017. Branched GDGT-based
832 paleotemperature reconstruction of the last 30,000 years in humid monsoon
833 region of Southeast China. *Chem. Geol.* 463, 94–102.
- 834 Weijers, J.W.H., Schouten, S., Spaargaren, O.C., Sinninghe Damsté, J.S., 2006.
835 Occurrence and distribution of tetraether membrane in soils: implications for the
836 use of the BIT index and the TEX₈₆ SST proxy. *Org. Geochem.* 37, 1680–1693.
- 837 Weijers, J.W.H., Schouten, S., van den Donker, J.C., Hopmans, E.C., Sinninghe
838 Damsté, J.S., 2007. Environmental controls on bacterial tetraether membrane lipid
839 distribution in soils. *Geochim. Cosmochim. Acta* 71, 703–713.
- 840 Wu, J.Y., Wang, Y.J., Dong, J., 2011. Changes in East Asian summer monsoon
841 during the Holocene recorded by stalagmite $\delta^{18}\text{O}$ records from Liaoning Province.
842 *Quat. Sci.* 31, 990–998 (in Chinese, with English abstract).
- 843 Xiao, J.L., Xu, Q.H., Nakamura, T., Yang, X.L., Liang, W.D., Inouchi, Y.W., 2004.
844 Holocene vegetation variation in the Daihai Lake region of north–central China:
845 a direct indication of the Asian monsoon climatic history. *Quat. Sci. Rev.* 23,

846 1669–1679.

847 Xie, S., Nott, C.J., Avsejs, L.A., Maddy, D., Chambers, F.M., Evershed, R.P., 2004.

848 Molecular and isotopic stratigraphy in an ombrotropic mire for palaeoclimate

849 reconstruction. *Geochim. Cosmochim. Acta*, 68, 2849–2862.

850 Xie S., Pancost R. D., Chen L., Evershed R. P., Yang H., Zhang K., Huang J. and Xu

851 Y. D., 2012. Microbial lipid records of highly alkaline deposits and enhanced

852 aridity associated with significant uplift of Tibetan Plateau in late Miocene.

853 *Geology* 40, 291–294.

854 Yamada, K., 2004. Last 40ka climate changes as deduced from the lacustrine

855 sediments of Lake Biwa, central Japan. *Quatern. Int.* 43-50, 123–125.

856 Yamamoto, S., Kawamura, K., Seki, O., Meyers, P. A., Zheng, Y. H., Zhou, W. J.,

857 2010. Environmental influences over the last 16ka on compound-specific $\delta^{13}\text{C}$

858 variations of leaf wax *n*-alkanes in the Hani peat deposit from northeast China.

859 *Chem. Geol.* 277, 261–268.

860 Yang, H., Pancost, R.D., Dang, X.Y., Zhou, X.Y., Evershed, R.P., Xiao, G.Q., Tang,

861 C.Y., Gao, L., Guo, Z.T., Xie, S.C., 2014. Correlations between microbial

862 tetraether lipids and environmental variables in Chinese soils: Optimizing the

863 paleo-reconstructions in semiarid and arid regions. *Geochim. Cosmochim. Acta*

864 126, 49–69.

865 Zhang, C.L., Pearson, A., Li, Y.L., Mills, G., Wiegand, J., 2006. Thermophilic

866 temperature optimum for crenarchaeol synthesis and its implication for archaeal

867 evolution. *Appl. Environ. Microb.* 72, 4419–4422.

868 Zhang, X., Jin, L., Huang, W., Chen, F., 2016. Forcing mechanisms of orbital-scale
869 changes in winter rainfall over northwestern China during the Holocene.
870 *Holocene* 26, 549–555.

871 Zhang, J.W., Chen, F.H., Holmes, J.A., Li, H., Guo, X.Y., Wang, J.L., Li, S., Lü, Y.B.,
872 Zhao, Y., Qiang, M.R., 2011. Holocene monsoon climate documented by oxygen
873 and carbon isotopes from lake sediments and peat bogs in China: a review and
874 synthesis. *Quat. Sci. Rev.* 30, 1973–1987.

875 Zhao, H., Chen, F.H., Li, S.H., Wintle, A.G., Fan, Y.X., Xia, D.S., 2007. A record of
876 Holocene climate change in the Guanzhong Basin, China, based on optical dating
877 of a loess–palaeosol sequence. *Holocene* 17, 1015–1022.

878 Zhao, H.L., Li, X.Q., Hall, V.A., 2015. Holocene vegetation change in relation to fire
879 and volcanic events in Jilin, Northeastern China. *Sci. China Earth Sci.* 58, 1404–
880 1419.

881 Zheng, Y., Zhou, W.J., Meyers, P.A., Xie, S., 2007. Lipid biomarkers in the
882 Zoigê-Hongyuan peat deposit: indicators of Holocene climate change in west
883 China. *Org. Geochem.* 38, 1927–1940.

884 Zheng, Y. H., Liu, X. M., Zhou, W. J., Zhang, C. L., 2011. *n*-Alkan-2-one distributions
885 in a northeastern China peat core spanning the last 16kyr. *Org. Geochem.* 42,
886 25–30.

887 Zheng, Y., Singarayer, J.S., Cheng, P., Yu, X., Liu, Z., Valdes, P.J., Pancost, R.D.,
888 2014. Holocene variations in peatland methane cycling associated with the Asian
889 summer monsoon system. *Nat. Commun.* 5, doi: 10.1038/ncomms5631.

890 Zheng, Y. H, Li, Q.Y., Wang, Z.Z., Naafs, D., Yu, X.F., Pancost, R.D., 2015.
891 Peatland GDGT records of Holocene climatic and biogeochemical responses to
892 the Asian Monsoon. *Org. Geochem.* 87, 86–95.

893 Zheng, Y., Pancost, R.D., Liu, X., Wang, Z., Naafs, B.D.A., Xie, X., Liu, Z., et al.,
894 2017. Atmospheric connections with the North Atlantic enhanced the deglacial
895 warming in northeast China. *Geology* 45, 1031–1034. doi: 10.1130/G39401.1.

896 Zhou, W.J., Lu, X.F., Wu, Z.K., Deng, L., Jull, A.J.T., Donahue, D., Beck, W., 2002.
897 Peat record reflecting Holocene climatic change in the Zoigê Plateau and AMS
898 radiocarbon dating. *Chinese Sci. Bull.* 47, 66–70.

899 Zhou, W. J. Yu, X.F., Jull, A.J.T., Burr, G., Xiao, J.Y., Lu, X.F., Xian, F., 2004.
900 High-resolution evidence from southern China of an early Holocene optimum
901 and a mid-Holocene dry event during the past 18,000 years. *Quat. Res.* 62, 39–
902 48.

903 Zhou, W., Song, S., Burr, G., Jull, A.J.T., Lu, X., Yu, H., Cheng, P., 2007. Is there a
904 time-transgressive Holocene Optimum in the East Asian monsoon area?
905 *Radiocarbon* 49, 865–875.

906 Zhou, W., Zheng, Y., Meyers, P.A., Timothy Jull, A.J., Xie, S., 2010. Postglacial
907 climate change record in biomarker lipid compositions of the Hani peat
908 sequence, Northeastern China. *Earth Planet. Sci. Lett.* 294, 37–46.

909 Zhou, X., Sun, L.G., Zhan, T., Huang, W., Zhou, X.Y., Hao, Q.Z., Wang, Y.H., He,
910 X.Q., Zhao, C., Zhang, J, Qiao, Y.S., Ge, J.Y., Yan, P., Yan, Q., Shao, D., Chu,
911 Z.D., Yang, W.Q., Smol, J.P., 2016. Time-transgressive onset of the Holocene

912 Optimum in the East Asian monsoon region. *Earth Planet. Sci. Lett.* 456, 39–46.
913 Zhu, C., Ma, C., Yu, S., Tang, L., Zhang, W., Lu, X., 2010. A detailed pollen record of
914 vegetation and climate changes in Central China during the past 16,000 years.
915 *Boreas* 39, 69–76.

916

917 **Figure captions**

918 **Figure 1:** Location of the Gushantun peat (yellow star) and other sites in arid central
919 Asia and the East Asian Monsoon region: Huguangyan Maar lake (Wang et al., 2007);
920 Dahu peat (Zhou et al., 2004); Dongge Cave (Dykoski et al., 2005); Dajiuhu peat
921 (Zhu et al., 2010); Sanbao Cave (Wang et al., 2008); Hongyuan peat (Zheng et al.,
922 2007); Yaoxian Loess (Zhao et al., 2007); Xunyi Loess (Stevens et al., 2008);
923 Luochuan Loess (Lu et al., 2013); Yulin Loess (Lu et al., 2013); Lake Dalianhai
924 (Cheng et al., 2013); Lake Qinghai (Shen et al., 2005; An et al., 2012; Wang et al.,
925 2014); Lake Gonghai (Chen et al., 2015); Lake Daihai (Xiao et al., 2004); Lake
926 Bayancha.(Bayanchagan, Jiang et al., 2006); Lake Tianchi (Zhou et al., 2016); Lake
927 Moon (Liu et al., 2010); Lake Sihailongwan (Stebich et al., 2015); Hani peat (Zhou et
928 al.,2010); Xinjiang loess (Chen et al., 2016); Bayanbulak (Long et al., 2017); Lake
929 Balikun (Tao et al., 2010); Lake Aibi (Wang et al., 2013); Lake Sayram (Jiang et al.,
930 2013); Lake Wulungu (Liu et al., 2008). Also shown are the dominant atmospheric
931 circulation systems: the EASM-East Asian summer monsoon, EAWM-East Asian
932 winter monsoon, WJ-Westerly jet.

933 **Figure 2:** The age-depth model of Gushantun peats using a Bacon-depth method.

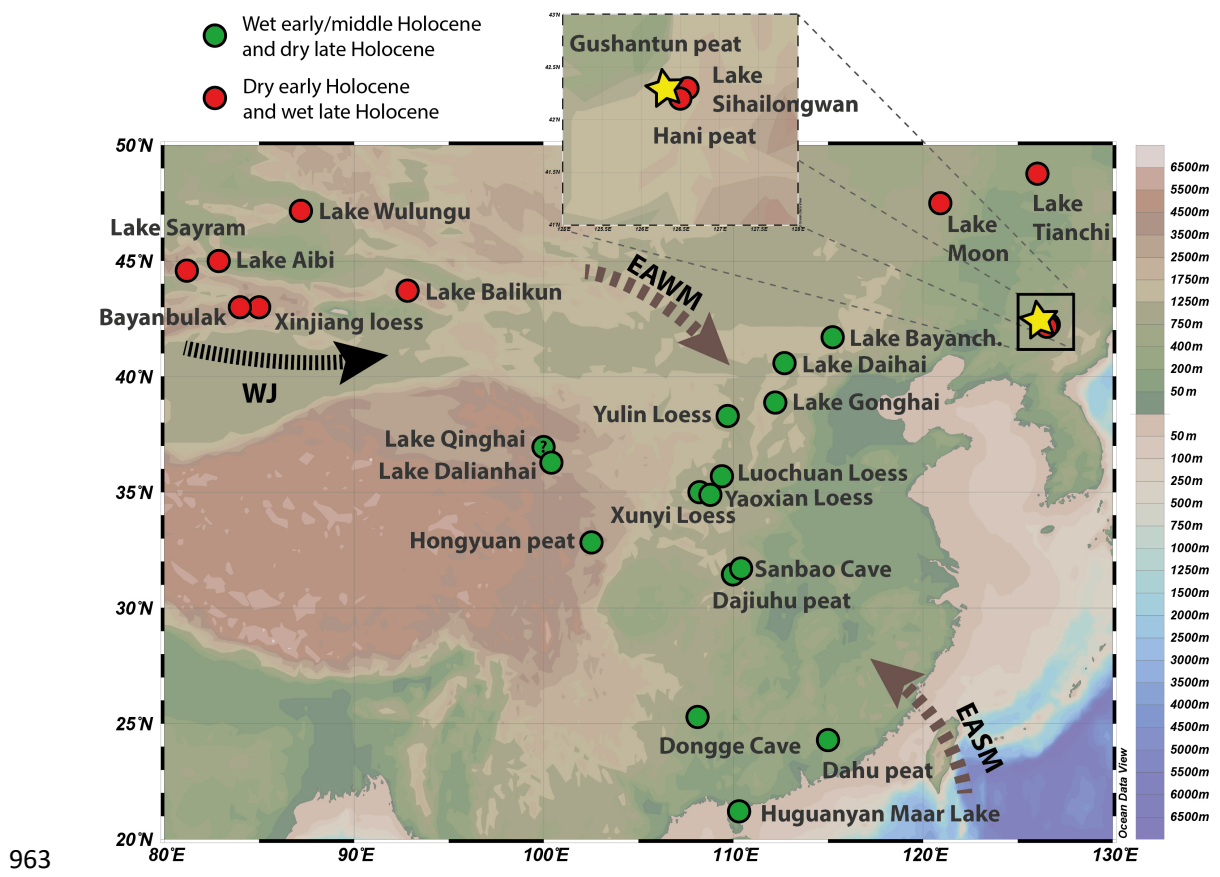
934 **Figure 3:** Comparison of reconstructed proxies based on brGDGTs in Gushantun peat
935 sequence with other temperature variations. (a). MAAT_{peat} variations in Gushantun
936 peat. The gray line is modern MAAT (~3 °C); (b). MAAT_{peat} variations in Hani peat
937 The gray line is modern MAAT (~5 °C) (Zheng et al., 2017); (c). A pollen-derived
938 mean warmest month (July) temperature changes (M_{twa}) of the Sihailongwan lake
939 sequence (Stebich et al., 2015). The gray bar shows lacustrine deposits at Gushantun
940 peat.

941 **Figure 4:** Reconstructed proxies in Gushantun peat sequence. (a). IR_{6me}; (b).
942 Fractional abundance of 6-methyl brGDGTs; (c). pH in Gushantun. The gray bar
943 shows lacustrine deposits at Gushantun peat.

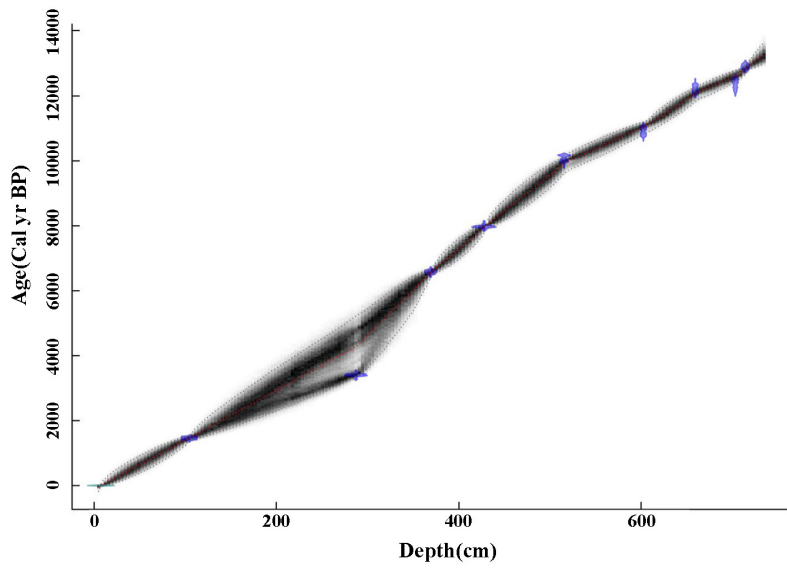
944 **Figure 5:** Comparison of Crenarchaeol and pH variations in Gushantun and Hani peat
945 sequence. (a) Crenarchaeol concentrations in Hani; (b). pH in Hani; (c). pH in
946 Gushantun; (d) Crenarchaeol concentrations in Gushantun.

947 **Figure 6:** Holocene moisture changes represented by pH in Gushantun peats and its
948 comparison with winter and summer insolation and other moisture changes from NE
949 China, the arid central Asia and other East Asian monsoon regions. (a) Northern
950 Hemisphere summer insolation (Berger and Loutre, 1991); (b) $\delta^{18}\text{O}$ record from
951 Dongge cave (Dykoski et al., 2005); (c) Pollen-based moisture index synthesized from
952 the East Asian summer monsoon rainfall belt over northern China (Wang and Feng,
953 2013); (d) EASM index synthesized from monsoonal eastern China (Wang et al.,
954 2010);(e) Northern Hemisphere winter insolation (Berger and Loutre, 1991); (f)
955 Strength of the westerlies represented by the winter insolation gradient between 35°

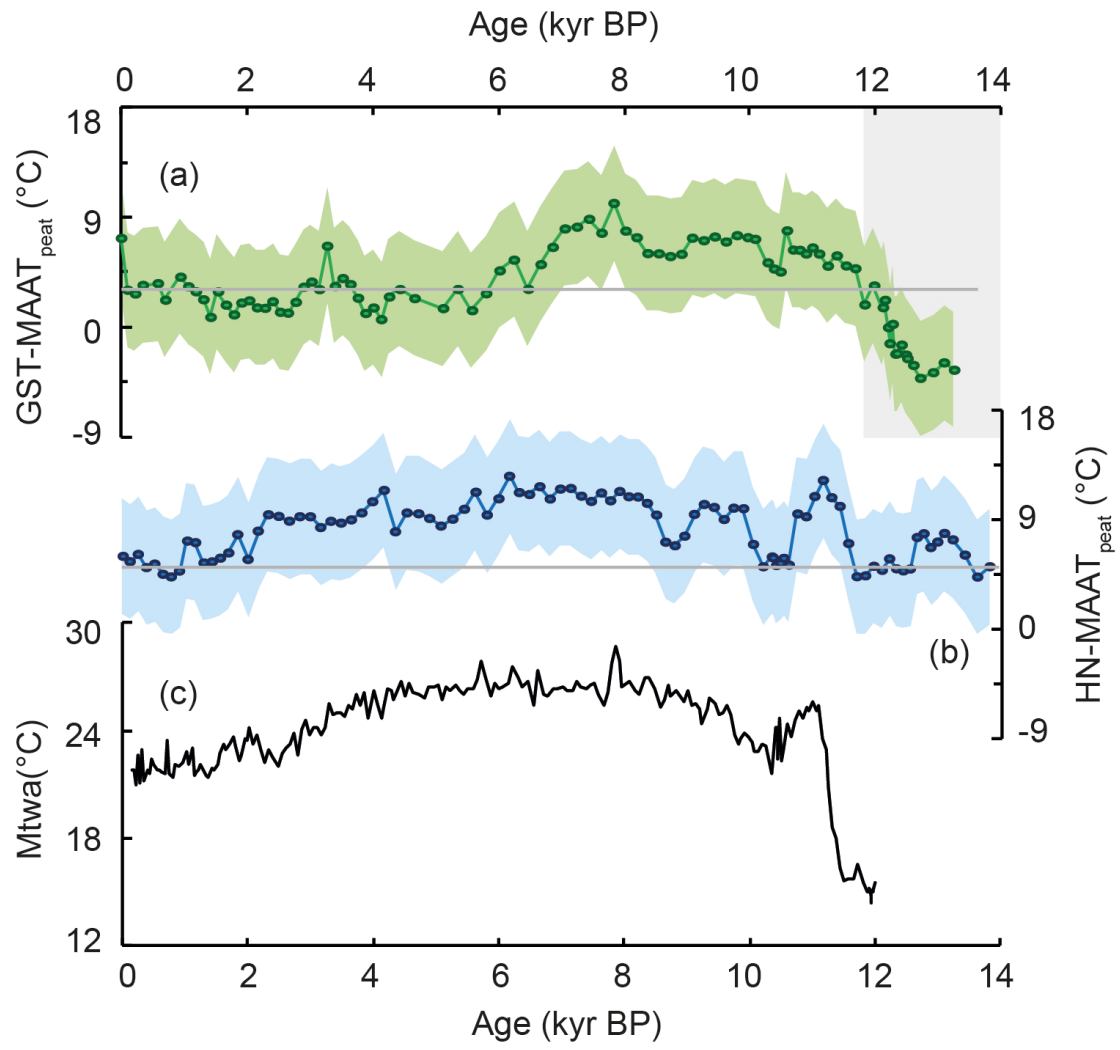
956 and 55°N (Rossby et al., 1939; Chen et al., 2016); (g) The tree pollen percentages in
 957 Tianchi lake (Zhou et al., 2016); (h) The pollen-derived Pann (mean annual
 958 precipitation) in Sihailongwan Maar lake (Stebich et al., 2015); (i) pH values from
 959 Gusnantun (this study; The black line is a polynomial regression trendline.); (j) The
 960 moisture changes from the LJW10 section of the Xinjiang Loess in the core area of
 961 Arid central Asia (Chen et al., 2016); (k) Synthesis of records of moisture variations
 962 in the Xinjiang region (Wang and Feng, 2013).



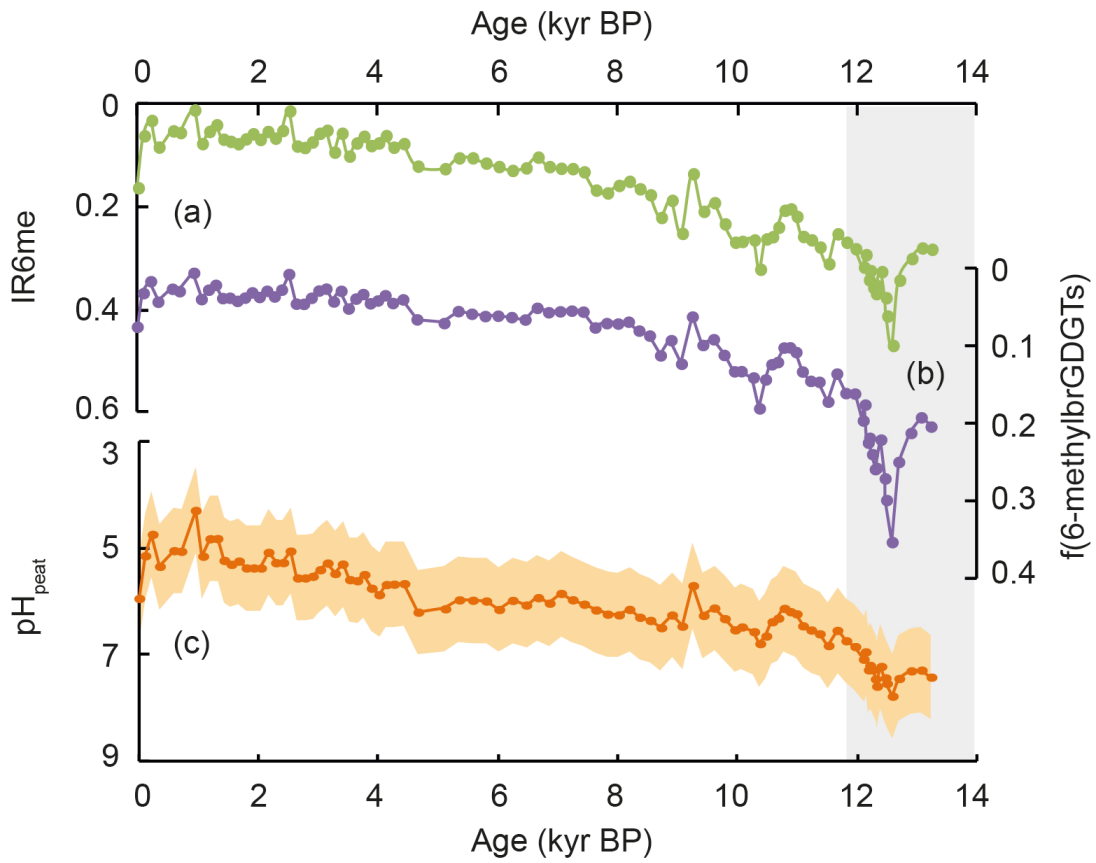
963



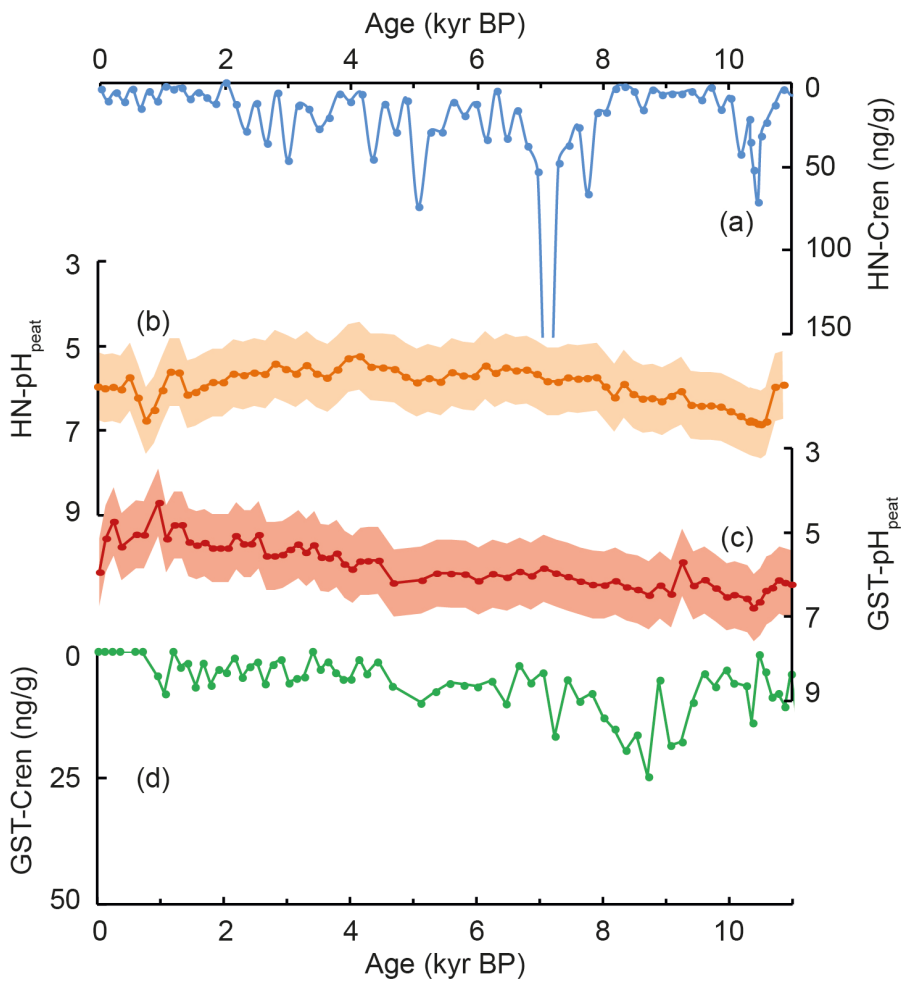
964



965



966



967

